

Infrared spectroscopy of small-molecule endofullerenes

T. Rõõm,^{1,*} L. Peedu,¹ Min Ge,¹ D. Huvonen,¹ U. Nagel,¹ S. Mamone,² M. H. Levitt,² M. Carravetta,² J. Y.-C. Chen,³ Xuegong Lei,³ N. J. Turro,³ Y. Murata,⁴ and K. Komatsu⁴

¹*National Institute of Chemical Physics and Biophysics,
Akadeemia tee 23, 12618 Tallinn, Estonia*

²*School of Chemistry, Southampton University,
Southampton SO17 1BJ, United Kingdom*

³*Department of Chemistry, Columbia University, New York, New York 10027, USA*

⁴*Institute for Chemical Research, Kyoto University, Kyoto 611-0011, Japan*

(Dated: February 12, 2019)

Hydrogen is one of the few molecules which has been incarcerated in the molecular cage of C_{60} and forms endohedral supramolecular complex $H_2@C_{60}$. In this confinement hydrogen acquires new properties. Its translational motion becomes quantized and is correlated with its rotations. We applied infrared spectroscopy to study the dynamics of hydrogen isotopologs H_2 , D_2 and HD incarcerated in C_{60} . The translational and rotational modes appear as side bands to the hydrogen vibrational mode in the mid infrared part of the absorption spectrum. Because of the large mass difference of hydrogen and C_{60} and the high symmetry of C_{60} the problem is identical to a problem of a vibrating rotor moving in a three-dimensional spherical potential. The translational motion within the C_{60} cavity breaks the inversion symmetry and induces optical activity of H_2 . We derive potential, rotational, vibrational and dipole moment parameters from the analysis of the infrared absorption spectra. Our results were used to derive the parameters of a pairwise additive five-dimensional potential energy surface for $H_2@C_{60}$. The same parameters were used to predict H_2 energies inside C_{70} [Xu et al., J. Chem. Phys., **130**, 224306 (2009)]. We compare the predicted energies and the low temperature infrared absorption spectra of $H_2@C_{70}$.

INTRODUCTION

A small cavity inside the fullerene cage is a potential trapping site of atoms and has attracted attention of scientists from the moment of discovery of C_{60} [1]. The demonstration of formation of $La@C_{60}$ after laser bombardment of La-impregnated graphite was immediate [2]. Since then the field of studies of endohedral fullerenes has expanded. Endohedral fullerenes with noble gas (He and Ne in [3], Ar, Kr, Xe [4]), nitrogen [5] or phosphorus [6] atoms and with metal clusters [7] are made under extreme conditions using arc discharge, ion bombardment or high pressure and high temperature treatment.

Extreme methods are not suitable for encapsulation of small molecules. A different approach, “chemical surgery”, was applied by Rubin when he made first open-cage fullerene [8] with a orifice large enough to load it with 3He or H_2 using less extreme temperature and pressure [9]. Soon Y. Murata, M. Murata and K. Komatsu synthesized another opened-cage derivative of C_{60} and achieved 100% yield in filling with H_2 [10]. There a generation of closed-cage $H_2@C_{60}$ was observed in the process of matrix-assisted laser desorption/ionization time-of-flight mass spectrometry analysis of this opened-cage complex. Chemical methods were developed to close opened-cage fullerenes and $H_2@C_{60}$ was produced in milligram quantities [11, 12]. To accommodate two hydrogen molecules a cavity larger than C_{60} is needed. Two H_2 were trapped in opened-cage C_{70} with the yield 3:97 in the favour of species with one H_2 per cage [13]. The restoration of closed cage retains approximately the same ratio of $(H_2)_2@C_{70}$ to $H_2@C_{70}$ [14]. Molecules other than hydrogen trapped in opened-cage fullerenes are carbon monoxide [15], water [16, 17], ammonia [18] and methane [19]. Recently Kurotobi and Murata succeeded in closing one of them and making the first closed-cage endohedral complex with a trapped polar molecule, $H_2O@C_{60}$ [20]. The rotational modes of endo-

hedral water were observed by inelastic neutron scattering (INS), far infrared (far-IR) and nuclear magnetic resonance (NMR) at cryogenic temperatures [21].

Up to date $\text{H}_2@C_{60}$ has been the most studied small molecule endofullerene. The local environment of a hydrogen molecule in the fullerene cage has a negligible inhomogeneous distribution of interaction parameters. All the trapping sites are similar in $\text{H}_2@C_{60}$, except the isotopic distribution of carbon atoms and crystal field effects in solid $\text{H}_2@C_{60}$. The $\text{H}_2@C_{60}$ is a stable complex and can survive a short period of heating up to 500 °C under vacuum [12]. These properties make $\text{H}_2@C_{60}$ appealing for spectroscopic and theoretical investigations of interactions between the molecular hydrogen and carbon nanosurfaces.

Three spectroscopic techniques NMR, INS and infrared (IR), have been used to study endohedral hydrogen. NMR studies cover spin lattice relaxation rates of $\text{H}_2@C_{60}$ in organic solvents [22, 23], and in the presence of paramagnetic relaxants [24, 25]. NMR was used to follow the *ortho-para* conversion in $\text{H}_2@C_{60}$ in the presence of molecular oxygen at 77 K [26] or upon photoexcitation of a C_{70} triplet state [27]. NMR study of micro-crystalline $\text{H}_2@C_{60}$ samples at cryogenic temperatures shows splitting of the $J = 1$ rotational state [28, 29], a sign of the symmetry reduction from the icosahedral symmetry in the solid phase. Similarly, splitting of the ground *ortho* state was deduced from the heat capacity measurements [30].

The overview of the low temperature NMR, INS and IR work on $\text{H}_2@C_{60}$ is given by Mamone et al. [31]. The first IR study of $\text{H}_2@C_{60}$ was limited to 6 K [32]. The translational and rotational transitions appeared as sidebands to the hydrogen molecule bond-stretching vibrational transition, $v = 0 \rightarrow 1$, in the mid-IR spectral range. The direct translational and rotational transitions were not observed in the far-IR below 200 cm^{-1} [33]. The extension of IR studies to higher temperature made possible to probe the hydrogen- C_{60} interaction potential in the ground $v = 0$ and first excited $v = 1$ vibrational states and a whole range of hydrogen isotopologs H_2 , D_2 and HD was studied [33, 34]. The isotope effects and translation-rotation coupling were also studied by INS in $\text{H}_2@C_{60}$ and HD@C_{60} [35]. The translational and rotational energies of $\text{H}_2@C_{60}$ and HD@C_{60} in the $v = 0$ state determined by IR spectroscopy are consistent with the low temperature INS results [35]. There is no Raman data on $\text{H}_2@C_{60}$, except a report on H_2 inside an opened-cage fullerene [36].

In this paper we will review the IR studies of hydrogen isotopologs in C_{60} and present the analysis of IR low temperature spectra of $\text{H}_2@C_{70}$. The far-IR properties of $\text{H}_2\text{O}@C_{60}$ will not be reviewed here [21].

THEORY

Quantum statistics plays an important role in the dihydrogen wavefunction symmetry and has a pronounced effect on the rotation of the hydrogen molecule [37]. The symmetry relative to the interchange of two protons dictates that there are two forms of molecular hydrogen, called *para*- and *ortho*- H_2 . The two proton spins ($I_p = 1/2$) are in the anti-symmetric $I = 0$ total nuclear spin state in *para*- H_2 and in the symmetric $I = 1$ state in *ortho*- H_2 . Even rotational quantum numbers J are allowed for *para*- H_2 and odd J for *ortho*- H_2 . The nucleus of D is a boson, nuclear spin $I_d = 1$. Thus the rotational state with an even quantum number J has D_2 in the state where the total nuclear spin of D_2 is either zero or two, $I = 0, 2$. This is called *ortho*- D_2 , while *para*- D_2 has the total nuclear spin $I = 1$ and odd J values.

A homonuclear diatomic molecule with the total nuclear spin $I = 1$ that is rotating in its ground state. This $J = 1$ rotational state is 118 cm^{-1} for H_2 , and 58 cm^{-1} for D_2 , above the rotational ground state $J = 0$ of even- I species. A thermal transition $J = 1 \rightarrow 0$ must be accompanied by the change of the total nuclear spin of the molecule, a process of very low probability. The time constant of thermal relaxation between the *ortho* and the *para* manifolds is very long and the room

The *ortho-para* ratio is maintained even at cryogenic temperatures. The equilibrium distribution of H₂ nuclear spin isomers is $n_o/n_p = 3$ and of D₂ is $n_o/n_p = 2$ at room temperature. To change the total nuclear spin of a molecule the two nuclei must experience different magnetic field. The *ortho-para* conversion can be activated by using a paramagnetic center as a source of the magnetic field gradient. The equilibrium $n_o/n_p = 1$ is reached at 77 K by dispersing H₂@C₆₀ on a zeolite surface and exposing it to molecular oxygen which acts like a spin catalyst [38]. There are no *ortho* and *para* species for HD. All rotational levels of HD are in thermal equilibrium and there is one rotational ground state, $J = 0$.

Quantum chemistry calculations are challenging for a hydrogen molecule in a weak van der Waals interaction with a large fullerene molecule. The availability of experimental data on endohedral H₂ has stimulated theoretical work in this direction. Theoretical investigations currently cover the calculations of rotation-translation energies of hydrogen isotopologs in C₆₀ [39, 40] and H₂ in C₇₀ [41], and the stability of C₆₀ or C₇₀ with one or more incarcerated H₂ [42, 43]. Empirical parameters of the Morse potential between H-H and contact Dirac interaction between H-C were adjusted [44] and density-fitting local Møller-Plesset theory tested [45] using the experimental H₂ vibrational frequency inside C₆₀. Classical molecular dynamics and density-functional theory have been combined to reproduce accurately the NMR chemical shift of ¹H in H₂@C₆₀ [46].

Both the hydrogen molecule and fullerene have closed shell electronic structures and therefore the interaction between them is the van der Waals interaction. The simplicity makes H₂@C₆₀ ideal for the studies of non-covalent bondings between H₂ and carbon nano-surfaces, the knowledge needed for the design of carbon-based hydrogen storage materials. The high icosahedral symmetry of the C₆₀ cavity is close to spherical and therefore H₂@C₆₀ represents a textbook example of a body moving in a spherical potential well [47, 48]. In addition, H₂ rotates around its center of mass. H₂ is not spherical and therefore its interaction with the walls of the cavity depends on its orientation what leads to the coupling between translational and rotational motion [49]. If the translational and the rotational motions are coupled then in the spherical potential the conserved angular momentum is the sum of translational and rotational angular momenta [39, 50]. H₂@C₆₀ is a rare example where the quantum dynamics of a diatomic rotor in a confined environment can be studied. Another, but with limited degrees of freedom, interesting example related to the fullerenes is the quantum rotor C₂ in a metallofullerene C₂@Sc₂C₈₄ [51, 52]. The two scandium atoms limit the translational motion and fix the rotational axis of C₂ relative to the fullerene cage. At low temperature the rotation of C₂ is hindered because it has a small rotational constant and is therefore more susceptible to the corrugations of the carbon surface. H₂ provides examples of two-dimensional rotors, like H₂ on a Cu surface [53] or H₂ in intercalated graphite [54].

High pressure loading of solid C₆₀ creates interstitial H₂. Exohedral H₂ has been studied by IR [55, 56], INS [57, 58], NMR [59, 60] and Raman [61] spectroscopies. Hydrogen is trapped in an interstitial site of octahedral symmetry and theory predicts translation-rotation coupling [50, 62]. However, broadening of experimental lines has prohibited accurate determination of the H₂-C₆₀ interaction potential.

The observed IR spectra of hydrogen encapsulated in C₆₀ consist of several absorption lines. We construct a model Hamiltonian and a dipole moment operator with few adjustable parameters to describe accurately the position and intensity of such multi-line spectrum.

Diatomic molecule in a spherical potential well

To describe the motion of a hydrogen molecule inside C₆₀ we use the following model. The C₆₀ is considered to be rigid, its center of mass is not moving and it does not rotate. We treat H₂@C₆₀ as an isolated molecular complex and approximate the true icosahedral symmetry of an isolated

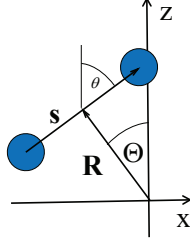


FIG. 1. Coordinates of a diatomic rotor inside the C_{60} cage are the relative position \mathbf{s} of two nuclei in the diatomic molecule and the diatomic center of mass displacement \mathbf{R} from the C_{60} cage center. In case of heteronuclear diatomic molecule (HD) the center of mass is not in the middle of the chemical bond between the two nuclei. Two polar spherical coordinates, Θ and θ , are shown. (Online version in Colour)

C_{60} with spherical symmetry. It means that in this approximation H_2 moves in a rigid spherically symmetric bounding potential provided by the cavity of C_{60} . Beside the translational movement inside C_{60} the hydrogen molecule has its internal degrees of freedom, vibration and rotation of two nuclei relative to its center of mass. There are no coupling terms between *ortho*- and *para*-states in our model Hamiltonian.

The theoretical work of Olthof et al. [63] is a comprehensive description of the dynamics of a loosely bound molecule inside C_{60} . Olthof et al. model the intermolecular potential as a sum of atom-atom potentials and expand it in spherical harmonics. They determined the radial part of the wavefunction with discrete variable representation method. The radial part of the wavefunction in our approach is given by algebraic functions, solution of the three-dimensional spherical oscillator [47, 48, 64]. The advantage is that matrix elements are calculated in algebraic form avoiding time-consuming numerical integration.

The position and orientation of the H_2 molecule is given by spherical coordinates $\mathbf{R} = \{R, \Omega\}$, $\Omega = \{\Theta, \Phi\}$ and $\mathbf{s} = \{s, \Omega_s\}$, $\Omega_s = \{\theta, \phi\}$ where \mathbf{R} is the vector from the center of the C_{60} cage to the center of mass of H_2 and \mathbf{s} is the internuclear H-H vector, as shown in Fig. 1. The center of mass translational motion of H_2 is given by eigenfunctions of the isotropic three-dimensional harmonic oscillator [48, 64]

$$\Psi_{NLM_L}^v(R, \Omega) = \psi_{NL}^v(R) Y_{LM_L}(\Omega), \quad (1)$$

where ψ_{NL}^v is the radial wave function and Y_{LM_L} is the spherical harmonic. The size of the H_2 molecule depends on its vibrational state $|v\rangle$. Therefore both, the bounding potential and $\psi_{NL}^v(R)$, depend on the vibrational quantum number v . The translational quantum numbers are $N = 0, 1, 2, \dots$. The orbital angular momentum quantum number takes values $L = N, N - 2, \dots, 1$ or 0, depending on the parity of N , and the azimuthal quantum number is $M_L = -L, -L + 1, \dots, L$. The rotational wavefunctions, defined by the rotational quantum numbers $J = 0, 1, \dots$ and $M_J = -J, -J + 1, \dots, +J$, are given by the spherical harmonics $Y_{JM_J}(\theta, \phi)$.

We use bipolar spherical harmonics with overall spherical rank Λ and component M_Λ

$$F_{\Lambda M_\Lambda}^{LJ}(\Omega, \Omega_s) = \sum_{M_L, M_J} \mathcal{C}_{LM_L JM_J}^{\Lambda M_\Lambda} Y_{LM_L}(\Omega) Y_{JM_J}(\Omega_s), \quad (2)$$

where \mathcal{C} are the Clebsch-Gordan coefficients [64]. Then the full wavefunction describing the motion of the H_2 molecule is

$$|vJNL\Lambda M_\Lambda\rangle = \psi_v^{vib}(s) \psi_{NL}^v(R) F_{\Lambda M_\Lambda}^{LJ}(\Omega, \Omega_s) \quad (3)$$

where $\psi_v^{vib}(s) \equiv |v\rangle$ is the vibrational wavefunction with the quantum number v .

The Hamiltonian \mathcal{H} for the trapped molecule includes coupling terms between vibrational, translational, and rotational motion. For simplicity, we neglect all matrix elements non-diagonal in v and introduce a parametric dependence on v ,

$$\mathcal{H} = {}^v\mathcal{H}^{\text{vib-rot}} + \frac{p^2}{2m} + {}^vV(R, \Omega, \Omega_s), \quad (4)$$

where ${}^v\mathcal{H}^{\text{vib-rot}}$ is the vibration-rotation Hamiltonian, p is the molecular momentum operator and m is the molecular mass of the diatomic molecule. ${}^vV = \langle v | V(R, s, \Omega, \Omega_s) | v \rangle$ is the potential energy of the hydrogen molecule in the vibrational state $\psi_v^{\text{vib}}(s)$. The vibration-rotation Hamiltonian ${}^v\mathcal{H}^{\text{vib-rot}}$ is diagonal in the basis set $|vJN\Lambda M_\Lambda\rangle$ with eigenvalues given by

$${}^vE_J^{\text{vib-rot}} = \hbar\omega_0(v + 1/2) + B_r J(J + 1), \quad (5)$$

$B_r = B_e - \alpha_e(v + 1/2) - D_e J(J + 1)$, where ω_0 is the fundamental vibrational frequency, α_e is the anharmonic correction and D_e is the centrifugal correction to the rotational constant B_e [65, 66].

We start from the general expansion of the potential in multipoles

$${}^vV(R, \Omega, \Omega_s) = \sum_{l,j,\lambda,m_\lambda} {}^vV_{\lambda m_\lambda}^{lj}(R) F_{\lambda m_\lambda}^{lj}(\Omega, \Omega_s). \quad (6)$$

and expand the radial part of potential ${}^vV_{\lambda m_\lambda}^{lj}(R)$ in powers of R

$${}^vV_{\lambda m_\lambda}^{lj}(R) = \sum_n {}^vV_{\lambda m_\lambda}^{ljn} R^n, \quad (7)$$

where $n \geq l$ and the parity of l and n is the same.

$V(\mathbf{R}, \mathbf{s})$ is a scalar and transforms under fully symmetric representation A_g of the symmetry group I_h . The spherical harmonics $\lambda = 0, 6, 10, \dots$ transform like A_g of the symmetry group I_h [67]. We use fully spherical approximation of the potential, $\lambda = 0$. Because $\lambda = 0$ and $\lambda = |l - j|, |l - j| + 1, \dots, l + j$ it must be that $l = j$.

The total potential is

$${}^vV = {}^vV_{00}^{000} F_{00}^{00} + ({}^vV_{00}^{002} R^2 + {}^vV_{00}^{004} R^4) F_{00}^{00} + ({}^vV_{00}^{111} R + {}^vV_{00}^{113} R^3) F_{00}^{11} + ({}^vV_{00}^{222} R^2 + {}^vV_{00}^{224} R^4) F_{00}^{22}, \quad (8)$$

if we limit our expansion to $j = l = 2$ and $n = 4$. The odd- j terms are not allowed by symmetry for H_2 and D_2 and thus the coefficients ${}^vV_{00}^{111}$ and ${}^vV_{00}^{113}$ are zero for homonuclear diatomic molecules.

If we set the constant off-set ${}^vV_{00}^{000} F_{00}^{00}$ to zero and write the perturbation part as

$${}^vV' = {}^vV_{00}^{004} R^4 F_{00}^{00} + ({}^vV_{00}^{111} R + {}^vV_{00}^{113} R^3) F_{00}^{11} + ({}^vV_{00}^{222} R^2 + {}^vV_{00}^{224} R^4) F_{00}^{22}, \quad (9)$$

and the isotropic harmonic term as ${}^vV^0 = {}^vV_{00}^{002} R^2 F_{00}^{00}$, then the total Hamiltonian reads

$$\mathcal{H} = {}^v\mathcal{H}^{\text{vib-rot}} + \frac{p^2}{2m} + {}^vV^0 + {}^vV'. \quad (10)$$

The unperturbed Hamiltonian eigenvalues in the basis $|vJN\Lambda M_\Lambda\rangle$ are

$$E_{vJN\Lambda M_\Lambda}^0 = {}^vE_J^{\text{vib-rot}} + \hbar v \omega_0^T (N + 3/2), \quad (11)$$

where $v \omega_0^T = ({}^vV_{00}^{002} / (2\pi m))^{1/2}$ is the frequency for translational oscillations within the cavity.

TABLE I. Translation-rotation energies of a 3D spherical oscillator $\langle vJNLA| \mathcal{H} - v\mathcal{H}^{\text{vib-rot}} |vJNLA\rangle$ for a perturbation given by Eq. 9 and \mathcal{H} by Eq. 10 for few lower states. Here $v\Delta^{004} = \frac{1}{v\beta} \frac{15}{8} \frac{vV_{00}^{004}}{vV_{00}^{002}}$, $v\Delta^{222} = \frac{\sqrt{5}}{20} \frac{vV_{00}^{222}}{vV_{00}^{002}}$, $v\Delta^{224} = \frac{1}{v\beta} \frac{7}{8\sqrt{5}} \frac{vV_{00}^{224}}{vV_{00}^{002}}$, and for $v\beta$ see Eq. 12.

$JNLA$	$\langle vJNLA \mathcal{H} - v\mathcal{H}^{\text{vib-rot}} vJNLA\rangle$
0000	$\hbar^v \omega_0^T [\frac{3}{2} + v\Delta^{004}]$
1001	$\hbar^v \omega_0^T [\frac{3}{2} + v\Delta^{004}]$
0111	$\hbar^v \omega_0^T [\frac{3}{2} + \frac{7}{3}v\Delta^{004}]$
1110	$\hbar^v \omega_0^T [\frac{5}{2} + \frac{7}{3}v\Delta^{004} + 10(v\Delta^{222} + v\Delta^{224})]$
1111	$\hbar^v \omega_0^T [\frac{5}{2} + \frac{7}{3}v\Delta^{004} - 5(v\Delta^{222} + v\Delta^{224})]$
1112	$\hbar^v \omega_0^T [\frac{5}{2} + \frac{7}{3}v\Delta^{004} + 1(v\Delta^{222} + v\Delta^{224})]$
2111	$\hbar^v \omega_0^T [\frac{5}{2} + \frac{7}{3}v\Delta^{004} + 5(v\Delta^{222} + v\Delta^{224})]$
2112	$\hbar^v \omega_0^T [\frac{5}{2} + \frac{7}{3}v\Delta^{004} - 5(v\Delta^{222} + v\Delta^{224})]$
2113	$\hbar^v \omega_0^T [\frac{5}{2} + \frac{7}{3}v\Delta^{004} + \frac{10}{7}(v\Delta^{222} + v\Delta^{224})]$
0200	$\hbar^v \omega_0^T [\frac{7}{2} + 5v\Delta^{004}]$
0222	$\hbar^v \omega_0^T [\frac{7}{2} + \frac{21}{5}v\Delta^{004}]$
1201	$\hbar^v \omega_0^T [\frac{7}{2} + 5v\Delta^{004}]$
1221	$\hbar^v \omega_0^T [\frac{7}{2} + \frac{21}{5}v\Delta^{004} + 7(v\Delta^{222} + \frac{9}{7}v\Delta^{224})]$
1222	$\hbar^v \omega_0^T [\frac{7}{2} + \frac{21}{5}v\Delta^{004} - 7(v\Delta^{222} + \frac{9}{7}v\Delta^{224})]$
1223	$\hbar^v \omega_0^T [\frac{7}{2} + \frac{21}{5}v\Delta^{004} + 2(v\Delta^{222} + \frac{9}{7}v\Delta^{224})]$

The meaning of different parts of the perturbation is explained by their influence on the energy levels of a harmonic 3D spherical oscillator, Table I. Translation-rotation coupling term vV_{00}^{222} splits energy of $|vJNLA\rangle$ state into levels with different Λ , where $\Lambda = |L - J|, |L - J| + 1, \dots, L + J$. For example, the $N = L = J = 1$ state is split into three levels with different total angular momentum $\Lambda = 0, 1, 2$. The ordering of levels depends on the sign of vV_{00}^{222} . The anharmonic correction to translation-rotation coupling is vV_{00}^{224} . If isotropic anharmonic correction vV_{00}^{004} is positive the distance between energy levels increases with N and this correction is different for the levels with same N but different L . For example, for positive vV_{00}^{004} the $N = 2, L = 0$ level has higher energy than $N = 2, L = 2$ level.

The length scale $v\beta = m^v \omega_0^T / \hbar$ (dimension m^{-2}) of the radial part of a 3D spherical oscillator wavefunction is related to the expectation value of the center of mass amplitude in state $|N\rangle$ as [47]

$$\langle N| R^2 |N\rangle = v\beta^{-2}(N + 3/2) = \hbar \sqrt{\frac{2\pi}{m^v V_{00}^{002}}}(N + 3/2). \quad (12)$$

Terms described by the translation-rotation coupling coefficients vV_{00}^{111} and vV_{00}^{113} do not appear in Table I because the first order correction to energies vanishes as the matrix element of F_{00}^{11} is zero if diagonal in L or J . These terms mix states with different N and J . For example, the first excited rotational state $J = 1, N = 0$ (expectation value of HD center of mass is on the cage center) has the state $J = 0, N = 1$ (expectation value of HD center of mass is off the cage center) mixed in [34]. The effect is that HD is forced to rotate about its geometric center instead of center of mass.

It was found by the 5D quantum mechanical calculation that the rotational quantum number J is almost a good quantum number for the homonuclear $\text{H}_2@\text{C}_{60}$ and $\text{D}_2@\text{C}_{60}$ and not for the heteronuclear $\text{HD}@\text{C}_{60}$ [40]. Indeed, vV_{00}^{22n} mixes states with different J for homonuclear species as well but the effect is reduced compared to the effect of vV_{00}^{11n} . In the former case $J \pm 2$ and $L \pm 2$

are mixed while in the latter case the $J \pm 1$ and $L \pm 1$ states that have a smaller energy separation are mixed.

The states with different Λ are not mixed in the spherical approximation, i.e. the total angular momentum $\mathbf{\Lambda} = \mathbf{L} + \mathbf{J}$ is conserved and Λ is a good quantum number. The other consequence of the spherical symmetry is that the energy does not depend on M_Λ . Therefore it is practical to use a reduced basis and reduced matrix elements [68] which are independent of M_Λ . This reduces the number of states by factor $2\Lambda + 1$ for each Λ .

Model Hamiltonian of $\text{H}_2@C_{70}$

A spherical approximation of the potential of a molecule trapped in C_{70} would be an oversimplification because of the elongated shape of C_{70} . The symmetry of C_{70} is D_{5h} , the distance between the centers of two capping pentagons (z direction) is 7.906 \AA . The diameter of the equatorial xy plane is 7.180 \AA [69], similar to the diameter of the icosahedral sphere of C_{60} , 7.113 \AA [70]. The anisotropy of the potential of H_2 inside C_{70} is supported by the 5D quantum mechanical calculation [41] what shows that the lowest translational excitation in the z direction is 54 cm^{-1} and in the xy plane is 132 cm^{-1} while in C_{60} it is 180 cm^{-1} and isotropic [33]. We derive from the IR spectra (see below) that the xy plane excitation energy is 151 cm^{-1} , somewhat larger than theoretically predicted.

Although the z axis translational energy in C_{70} is three times less than in the icosahedral C_{60} , the effect of the C_{70} potential on the rotational motion is moderate. The splitting of the $J = 1$ state is 7 cm^{-1} what is relatively small compared to the rotational energy 120 cm^{-1} in this state [41].

To analyze the IR spectra of $\text{H}_2@C_{70}$ we use a simplified Hamiltonian where the translational energy is represented in the form of the sum of two oscillators, 1D linear and 2D circular oscillator, and we do not consider anharmonic corrections and the translation-rotation coupling.

The vibration-rotation energy

$${}^v E_{JJ_z}^{\text{vib-rot}} = \hbar \omega_0 \left(v + \frac{1}{2} \right) + B_r^{(v)} J(J+1) + {}^v \kappa (3J_z^2 - 2), \quad (13)$$

is the same as for $\text{H}_2@C_{60}$ except the last term which accounts for the axial symmetry of the C_{70} potential with the rotational anisotropy parameter ${}^v \kappa$ [71]. For example, the three-fold degenerate $J = 1$ rotational state in I_h symmetry is split in D_{5h} symmetry and if ${}^v \kappa > 0$ the $J_z = 0$ state is $3{}^v \kappa$ below the twice degenerate $J_z = \pm 1$ rotational state.

The translational part is added to the vibration-rotation Hamiltonian, Eq.13, and the total energy reads

$$E_{vJJ_z;nl n_z}^0 = {}^v E_{JJ_z}^{\text{vib-rot}} + \hbar {}^v \omega_{xy}^T (n+1) + \hbar {}^v \omega_z^T \left(n_z + \frac{1}{2} \right). \quad (14)$$

Here the translational energy is written as a sum of two oscillators, a linear oscillator along the z axis with translational quantum $\hbar {}^v \omega_z^T$ and a 2D (circular) oscillator [48, 64] in the xy plane with translational quantum $\hbar {}^v \omega_{xy}^T$. Quantum numbers n_z and n are positive integers including zero and $l = n, n-2, \dots, -n+2, -n$.

We will show below that the frequencies of z and xy translational modes, ${}^1 \omega_z^T$ and ${}^1 \omega_{xy}^T$, can be determined from the experimental data even though the translation-rotation coupling is not known. We take the advantage of translation-rotation coupling being zero in the $J = 0$ rotational state. The complication rises from the fact that the potential is different in the initial and final states of the IR transitions, $v = 0$ and 1. However, this complication could be resolved if the energy of the fundamental vibrational transition $v = 0 \rightarrow 1$ (without change of n and n_z) is known.

TABLE II. Classification of energy levels of H₂ inside the cage of C₇₀ up to $J = 1$ and $n = n_z = 1$ by irreducible representations Γ_i of the symmetry group D_{5h} .

J	$(nl n_z)$	Γ_i
0	(000)	A'_1
1	(000)	A''_2, E'_1
0	(001)	A''_2
1	(001)	A'_1, E''_1
0	(110)	E''_1
1	(110)	A'_1, A'_2, E'_2, E''_1

The $\Delta J = 0$ transition from the *para*-H₂ ground state leads to two excitation energies in the IR spectrum, one for the z mode and second for the xy mode

$$E_{100;001}^0 - E_{000;000}^0 = \hbar[\omega_0 + {}^1\omega_z^T + ({}^1\omega_{xy}^T - {}^0\omega_{xy}^T) + \frac{1}{2}({}^1\omega_z^T - {}^0\omega_z^T)], \quad (15)$$

$$E_{100;110}^0 - E_{000;000}^0 = \hbar[\omega_0 + {}^1\omega_{xy}^T + ({}^1\omega_{xy}^T - {}^0\omega_{xy}^T) + \frac{1}{2}({}^1\omega_z^T - {}^0\omega_z^T)]. \quad (16)$$

Defining the fundamental *para* transition energy as $E_{100;000}^0 - E_{000;000}^0 = \hbar[\omega_0 + ({}^1\omega_{xy}^T - {}^0\omega_{xy}^T) + \frac{1}{2}({}^1\omega_z^T - {}^0\omega_z^T)]$ we may rewrite Eq. 15 and 16 as

$$\begin{aligned} E_{100;001}^0 - E_{000;000}^0 &= \hbar{}^1\omega_z^T + E_{100;000}^0 - E_{000;000}^0, \\ E_{100;110}^0 - E_{000;000}^0 &= \hbar{}^1\omega_{xy}^T + E_{100;000}^0 - E_{000;000}^0. \end{aligned} \quad (17)$$

From these equations translational frequencies in the excited $v = 1$ state, ${}^1\omega_z^T$ and ${}^1\omega_{xy}^T$, can be determined without knowing the translation-rotation coupling.

The classification of energy levels up to $J = 1$ and $n = n_z = 1$ by irreducible representations Γ_i of the symmetry group D_{5h} is given in Table II. We get the irreducible representations Γ_j : $L = 0 \rightarrow A'_1$ and $L = 1 \rightarrow A''_2 + E'_1$ by subducting the translational states represented by spherical harmonics Y_{LM_L} from the full rotational group $O(3)$ to the symmetry group D_{5h} . A'_1 is the *para*-H₂ ground state, $n = l = n_z = 0$. The first excited state of the z mode is $n_z = 1$ and A''_2 . The first excited state of the xy mode $n = l = 1$ is doubly degenerate E'_1 . The full symmetry when translations and rotations are taken into account is $\Gamma_i = \Gamma_j \otimes \Gamma^{(J)}$. For example, the *ortho*-H₂ ground state, $J = 1$ and $(nl n_z) = (000)$, is split into $J_z = 0$ (A''_2) and $J_z = \pm 1$ (E'_1), see Table II.

Induced dipole moment of hydrogen in spherical environment

IR light is not absorbed by vibrations and rotations of homonuclear diatomic molecules [65]. IR activity of H₂ is induced in the presence of intermolecular interactions, such as in the solid and liquid phases [72, 73], in constrained environments [55, 56, 62, 74], and in pressurized gases [75, 76]. IR spectra of such systems are usually broad due to inhomogeneities in the system or due to random molecular collisions. As an exception, narrow lines are observed in semiconductor crystals [77] and solid hydrogen [78].

An overview of collision-induced dipoles in gases and gas mixtures is given in the book by L. Frommhold [79]. The confinement of the endohedral H₂ introduces two differences as compared to H₂ in the gas. *First*, the translational energy of H₂ is quantized. In the gas phase it is a continuum starting from zero energy. *Second*, the variation of the distance between H₂ and the carbon atom is limited to the translational amplitude of H₂ in the confining potential. In the gas phase the distance varies from infinity to the minimal distance given by the collision radius. The selection rule $\Delta N = \pm 1$ for the endohedral H₂ follows from these two conditions, as shown below.

Quantum mechanical calculations of induced dipoles are available for simple binary systems like H₂-He, H₂-Ar, and H₂-H₂. An extensive set of theoretical results for the H₂-He system associated with the roto-translation electric dipole transitions, both in the vibrational ground state $v = 0$ and accompanying the $v = 0 \rightarrow 1$ transition of the H₂ molecule, can be found in [80–84]. Related to the fullerene studies are calculations of the dipole moment of CO@C₆₀ [63] and exohedral H₂ in solid C₆₀ [62].

We express the induced part of the dipole moment as an interaction between hydrogen molecule and C₆₀. Another approach was used in [33] where the summation over 60 pair-wise induced dipole moments between H₂ and carbon atoms was done. The relation between two sets of parameters was given [34].

We write the expansion of the dipole moment from the vibrational state v to v' in bipolar spherical harmonics and in power series of R as

$$d_{v'v}(\mathbf{R}, \Omega_s) = \frac{4\pi}{\sqrt{3}} \sum_{l,j,n} v'v A_{\lambda m_\lambda}^{l j n} R^n F_{\lambda m_\lambda}^{l j}(\Omega, \Omega_s). \quad (18)$$

This is similar to the expansion of the potential discussed above, except the dipole moment is a polar vector while the potential is a scalar. The dipole moment transforms according to the irreducible representation T_{1u} of the symmetry group I_h . The spherical harmonics of the order $\lambda = 1, 5, 7, \dots$ transform according to T_{1u} of the symmetry group I_h [67]. We use $\lambda = 1$ and are interested in $v = 0 \rightarrow 1$ transitions. In spherical symmetry it is sufficient to calculate one component of the dipole moment vector, $m_\lambda = 0$, and if we drop the explicit dependence of $d_{v'v}$ on v, v' and of $v'v A_{\lambda m_\lambda}^{l j n}$ on λ, m_λ , the $m_\lambda = 0$ component of the dipole moment reads

$$d_0(\mathbf{R}, \Omega_s) = \frac{4\pi}{\sqrt{3}} \sum_{l,j,n} A^{l j n} R^n F_{10}^{l j}(\Omega, \Omega_s). \quad (19)$$

As $\lambda = |l - j|, |l - j| + 1, \dots, l + j$ and $\lambda = 1$ it must be that $l = |j \pm 1|$. The possible combinations are $(lj) \in \{(01), (10), (12), (21), (23), \dots\}$. If we restrict the expansion up to $n = l = 1$, we get

$$d_0(\mathbf{R}, \Omega_s) = \frac{4\pi}{\sqrt{3}} A^{010} F_{10}^{01} + \frac{4\pi}{\sqrt{3}} (A^{101} F_{10}^{10} + A^{121} F_{10}^{12}) R.$$

A^{010} is zero for homonuclear diatomic molecules H₂ and D₂. It is the sum of the HD permanent rotational dipole moment in the gas phase and the induced rotational dipole moment inside C₆₀. The selection rule is $\Delta N = 0, \Delta J = 0, \pm 1$, but $J = 0 \rightarrow 0$ is forbidden.

The expansion coefficients A^{101} and A^{121} are allowed by symmetry for both, homo- and heteronuclear diatomic molecules. The expansion coefficient A^{101} describes the induced dipole moment that is independent of the orientation of the diatomic molecular axis \mathbf{s} , selection rule $\Delta N = 0, \pm 1, \Delta J = 0$, but $N = 0 \rightarrow 0$ is forbidden. A^{121} describes the induced dipole moment that depends on the orientation of \mathbf{s} , $\Delta N = 0, \pm 1, \Delta J = 0, \pm 2$, but $N = 0 \rightarrow 0$ and $J = 0 \rightarrow 0$ are both forbidden. All terms in Eq. 20 satisfy the selection rule $\Delta \Lambda = 0, \pm 1$, but $\Lambda = 0 \rightarrow 0$ is forbidden.

Although HD has a permanent rotational dipole moment, the induced dipole moment dominates inside C₆₀ [34].

IR absorption line intensity [33] is proportional to the thermal population of the initial state. If the thermal relaxation between *para*-H₂ and *ortho*-H₂ is very slow we can define a temperature independent fractional *ortho* and *para* populations n_k of the total number of molecules \mathcal{N} , where $k = o, p$ selects *ortho* or *para*-H₂. Then the probability that the initial state $|v_i J_i N_i L_i \Lambda_i M_{\Lambda_i}\rangle$ is populated is

$$p_i = n_k \frac{e^{-E_i/k_B T}}{\sum_j g_j e^{-E_j/k_B T}}, \quad (20)$$

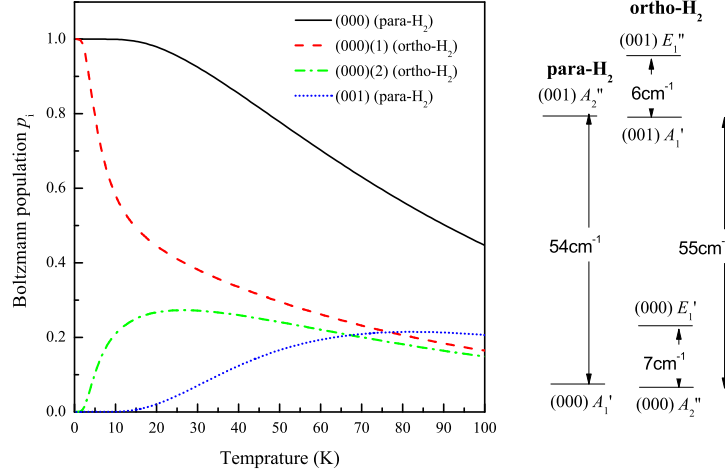


FIG. 2. Boltzmann population of the $\text{H}_2@C_{70}$ *para* ground translational state (000)(solid line) and first thermally excited (dotted line) state (001) and of the two *ortho* states, A_2'' (dashed line) and E_1'' (dash-dot line), in the ground translational state (000), calculated using energy levels of the 5D quantum mechanical calculation [41]. Here the *para* states have $J = 0$ and the *ortho* states have $J = 1$; irreducible representations are from Table II. (Online version in Colour)

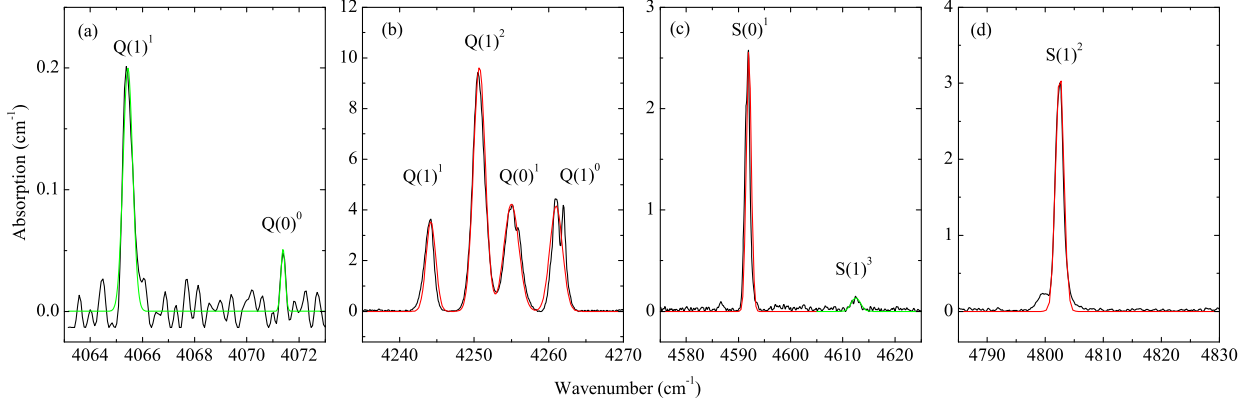


FIG. 3. Infrared absorption spectra of $\text{H}_2@C_{60}$ at 6 K are shown with the black line. The green line in panel (a) is the Gaussian fit of fundamental *para* and *ortho* transitions, $\Delta N = \Delta J = 0$. The red line in panels (b), (c), (d) is the simulated spectrum with parameters taken from the model fit of 200 K spectra [33]. The $S(1)^3$ labeled green line in panel (c) is the Gaussian fit of the $\Delta N = 0, \Delta J = 2$ forbidden *ortho* transition, experimentally observed at 4612.5 cm^{-1} and predicted to be at 4613.1 cm^{-1} by our model [33]. Line labels are the same as in Fig. 4a; the superscript to line label shows the final state Λ .

where E_i is the energy of the initial state measured from the ground state $v = N = 0$ and j runs over all *para*- (or *ortho*-) H_2 states in the basis used. $g_j = 2\Lambda_j + 1$ is the degeneracy of the energy level E_j . Please note that g_i does not appear in the numerator because p_i is the population of a individual state $|v_i J_i N_i L_i \Lambda_i M_{\Lambda_i}\rangle$ although the reduced basis $|v J N L \Lambda\rangle$ is used. Hetero-nuclear HD has no *para* and *ortho* species and the coefficient n_k in Eq. 20 must be set to one, $n_k = 1$.

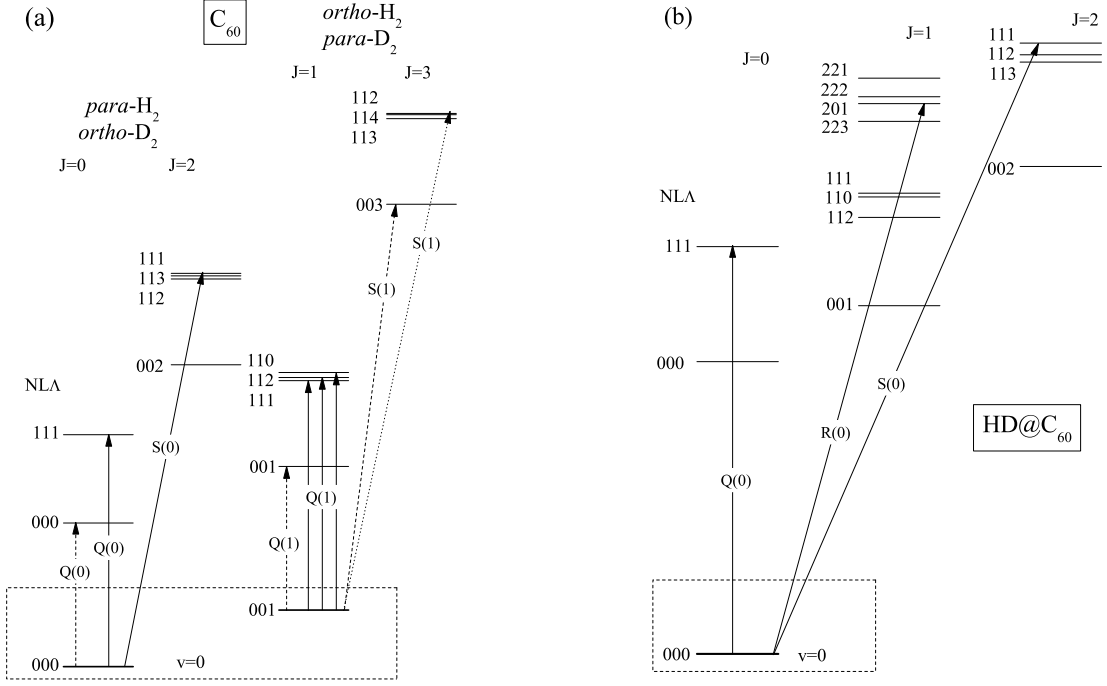


FIG. 4. Diagrams of the observed low temperature IR transitions in hydrogen isotopologs (a) H_2 , D_2 and (b) HD incarcerated in C_{60} . The initial states surrounded by a dashed box have the vibrational quantum number $v = 0$; all the final states are in the excited vibrational state $v = 1$. Dashed lines in (a) are forbidden transitions ($\Delta N = 0$) that are observed in $\text{H}_2@C_{60}$ but not in $\text{D}_2@C_{60}$. The S(1) line (dotted) with $\Delta N = 1$ is not observed in $\text{D}_2@C_{60}$. The line label $Q(J_i)$ is used for $\Delta J = 0$, $R(J_i)$ is used for $\Delta J = +1$ and $S(J_i)$ for $\Delta J = +2$ transitions where J_i is the initial state J .

Infrared absorption by $\text{H}_2@C_{70}$

The infrared absorption in $\text{H}_2@C_{70}$ is given by electric dipole operators d_0 and $d_{\pm 1}$, which transform like A_2'' and E_1' irreducible representations of D_{5h} . At low T the symmetry-allowed transitions from the ground *para* state are $A_1' \xrightarrow{d_0} A_2''$ and $A_1' \xrightarrow{d_{\pm 1}} E_1'$. Two *ortho* states, A_2'' and E_1' , are populated at low T , Fig. 2. The transitions are $A_2'' \xrightarrow{d_0} A_1'$ and $A_2'' \xrightarrow{d_{\pm 1}} E_1''$. The symmetry-allowed transitions from the E_1' state are $E_1' \xrightarrow{d_0} E_1''$ and $E_1' \xrightarrow{d_{\pm 1}} A_1', A_2', E_2'$.

The IR absorption line area is proportional to the Boltzmann population of the initial state, Eq. 20. The degeneracy g_j of the energy level E_j is one or two in case of $\text{H}_2@C_{70}$. Fig. 2 shows the Boltzmann population of the few first *para* and *ortho* levels in the $v = 0$ vibrational state. The *para* state (000) population (solid line) starts to drop above 20 K as the first excited state (001) (black dashed line) at 54 cm^{-1} above the ground state becomes populated and drains the population from the (000) state. The abrupt change of the population of *ortho* ground states above 2 K is because of the transfer of population from the non-degenerate A_2'' ground level (dotted line) to the doubly degenerate E_1' (dash-dot line) 7 cm^{-1} higher. The populations of A_2'' and E_1' states decrease above 30 K as the first excited translational (001) *ortho* state get more populated.

EXPERIMENT

The endohedral complexes were prepared by “molecular surgery” as described in [11, 12]; $\text{H}_2@C_{60}$, $\text{D}_2@C_{60}$ and $\text{H}_2@C_{70}$ at Kyoto University, and $\text{HD}@C_{60}$ at Kyoto University and Columbia University. The $\text{HD}@C_{60}$ sample was a mixture of the hydrogen isotopomers $\text{H}_2:\text{HD}:\text{D}_2$ with the ratio 45:45:10. Since all C_{60} cages are filled, the filling factor for HD is $\rho = 0.45$. The content of C_{70} sample was empty: $\text{H}_2:(\text{H}_2)_2=28:70:2$ and the filling factor $\rho = 0.7$. Experimental absorption spectra were corrected for the filling factor.

The *para* enriched sample was made at Columbia University using molecular oxygen as a spin catalyst for *ortho-para* conversion [26]. Briefly, the $\text{H}_2@C_{60}$ adsorbed on the external surface of NaY zeolite was immersed in liquid oxygen at 77 K for 30 minutes, thereby converting the incarcerated H_2 spin isomers to the equilibrium distribution at 77 K, $n_o/n_p = 1$. The liquid oxygen was pumped away and the endofullerene-NaY complex was brought back rapidly to room temperature. The *para* enriched $\text{H}_2@C_{60}$ was extracted from the zeolite with CS_2 and the solvent was evaporated by argon. The powder sample in argon atmosphere and on dry ice arrived in Tallinn four days after the preparation.

Powdered samples were pressed under vacuum into 3 mm diameter pellets for IR transmission measurements. Typical sample thickness was 0.3 mm. Two identical vacuum tight chambers with Mylar windows were employed in the IR measurements. The chambers were put inside an optical cold finger type cryostat with KBr windows. In the measurements, the chamber containing the pellet for analysis was filled with He exchange gas while the empty chamber served as a reference. Transmission spectra were obtained using a Bruker interferometer Vertex 80v with a halogen lamp and a HgCdTe or an InSb detector. The apodized resolution was typically 0.3 cm^{-1} or better.

Transmission $T_r(\omega)$ was measured as the light intensity transmitted by the sample divided by the light intensity transmitted by the reference. The absorption coefficient $\alpha(\omega)$ was calculated from the transmission $T_r(\omega)$ through $\alpha(\omega) = -d^{-1} \ln [T_r(\omega)(1 - R)^{-2}]$, with the reflection coefficient $R = [(\eta - 1)/(\eta + 1)]^2$ calculated assuming a frequency-independent index of refraction [85], $\eta = 2$. Absorption spectra were cut into shorter pieces around groups of H_2 lines and a baseline correction was performed before fitting the H_2 lines with Gaussians.

RESULTS AND DISCUSSION

C_{60}

The IR absorption spectra of $\text{H}_2@C_{60}$ at 6 K together with the simulated spectra are shown in Fig. 3 and the diagram of energy levels involved in Fig. 4a. The simulated spectra are calculated using Hamiltonian, dipole moment and the *ortho-para* ratio parameters (see Table IV) obtained from the fit of 200 K spectra [33]. Temperature does not affect these parameters and the line intensities follow the Boltzmann population of initial states [33]. Intensity of three lines, $Q(0)^0$ and $Q(1)^1$ in Fig. 3 a) and $S(1)^3$ in c) can not be simulated because the induced dipole moment theory does not describe $\Delta N = 0$ transitions. However, the position of these three lines was used to fit the Hamiltonian parameters [33]. The splitting of the *ortho* state $N = J = 1$ into $\Lambda = 0, 1$ and 2 by translation-rotation coupling is seen in Fig. 3 b). The *para* $N = 1, J = 2$ and *ortho* $N = 1, J = 3$ states are split into three sublevels as well. However, because of the selection rule $\Delta\Lambda = \pm 1$ only one *para* and one *ortho* S -transition is IR active.

The intensity of other lines in Fig. 3 b-d) is described accurately by two dipole moment parameters, A^{101} and A^{121} , and *ortho-para* ratio $n_o/n_p = 2.89 \pm 0.045$, what is very close to the statistical value three, Table IV. We confirmed the assignment of spectral lines to *para*- and *ortho*- H_2 by

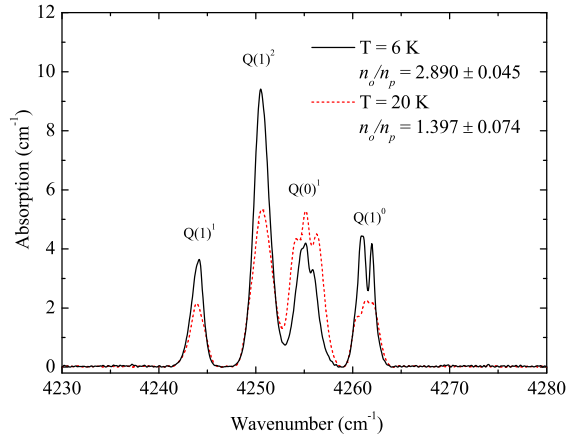


FIG. 5. Spectra in the region of Q lines of a *para* enriched $\text{H}_2@C_{60}$ (dashed line) and non-enriched sample (solid line) at low T . The thermal equilibrium *ortho-para* ratio at 78 K where the *para* enrichment was done is $n_o/n_p = 1$. (Online version in Colour)

measuring the spectrum of a *para* enriched $\text{H}_2@C_{60}$ sample [33]. Low T spectra in the region of Q lines are shown in Fig. 5. The time delay between *para* enrichment and first IR measurement was 4 days. The 4255 cm^{-1} *para* line is stronger and other three *ortho* lines are weaker in the *para*-enriched sample, as compared to the non-enriched sample.

The Fig. 5 deserves some attention. Lines $Q(0)^1$ and $Q(1)^0$ have a clear multicomponent structure and it is different for the two samples. This is not possible in the approximation of spherical symmetry. Even not by considering the true icosahedral symmetry of C_{60} because the lowest Λ value for the state which is split by the icosahedral symmetry is three while the initial and final states of the optical transitions under discussion have only $\Lambda = 0, 1$. Later measurements on the relaxed but initially *para* converted sample showed that the difference between the line shapes of the normal and *para* converted sample is not due to the different *ortho-para* ratio. Thus it is likely that the difference in the line splitting is due to a different impurity content of the two samples. However, it is not completely excluded that the crystal field or the distortion of the C_{60} cage is responsible for the part of this splitting. Note that the $Q(1)^0$ line of $\text{D}_2@C_{60}$, Fig. 6, bears similar splitting pattern as in $\text{H}_2@C_{60}$.

The $\text{D}_2@C_{60}$ spectrum, Fig. 6, is shifted to lower frequency compared to $\text{H}_2@C_{60}$ because of the heavier mass of D_2 . The spectrum has less lines than the $\text{H}_2@C_{60}$ spectrum. The missing transitions in $\text{D}_2@C_{60}$ are shown in red color in Fig. 4a and they belong to J -odd species which are minority for D_2 .

The splitting of $N = J = 1$ into $\Lambda = 0, 1$ and 2 states is similar in D_2 and H_2 . The magnitude of the splitting, $\hbar^2 \omega_0^T \frac{\sqrt{5}}{20} \frac{vV_{00}^{222}}{vV_{00}^{002}}$, see Table I, is less in D_2 because ${}^1\omega_0^T$ is smaller although ${}^1V_{00}^{002}$ and ${}^1V_{00}^{222}$ are similar for two isotopologs, Table IV. Line $Q(1)^2$ overlaps partially with $Q(0)^1$ line, Fig. 6. However, this is not because the translation-rotation splitting is different for two isotopologs but because of a smaller anharmonic correction α_e of the rotational constant for D_2 , Table IV.

The spectrum of $\text{HD}@C_{60}$ is more simple, Fig. 7, because there are no *para* and *ortho* species and therefore only one state is populated at low T . There is one spectral line, not present in homonuclear dihydrogen, labeled $R(0)$ in Fig. 4b and Fig. 7. HD has no inversion symmetry and the ban on $\Delta J = 1$ transitions is lifted. The classification of this transition as $\Delta J = 1$ is arbitrary first, because the weight of $JN\Lambda = 1201$ is only 0.5 in this state [34] and secondly, the change of translational state is $\Delta N = 2$, not allowed by any of the dipole operator components in our model. The next component in weight 0.29 in the final state is $JN\Lambda = 2111$ which makes this transition

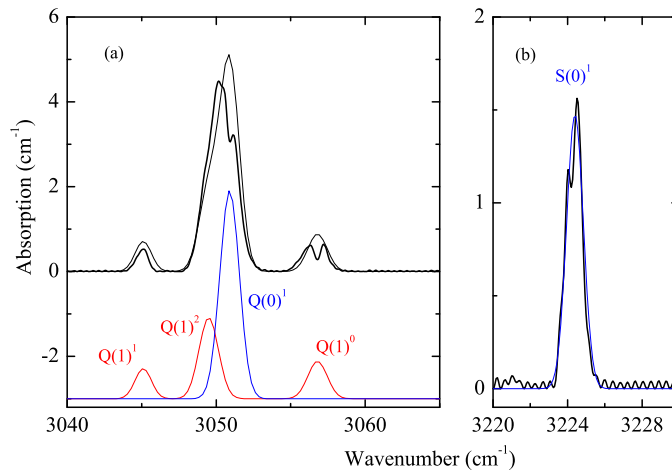


FIG. 6. Infrared absorption spectra of $D_2@C_{60}$ at 5 K. The simulated spectrum is shown by red line (*para*), blue line (*ortho*) and black thin line (sum of *para* and *ortho* spectra). The parameters for the simulated spectrum are taken from the model fit of the 90 K spectrum [34]. Line labels are the same as in Fig. 4a; superscript to line label shows the final state Λ .

A^{121} -active, $N = 0 \rightarrow 1, J = 0 \rightarrow 2$ and therefore it would be more appropriate to classify it as an S line. Another interesting feature of the HD spectrum is the absence of $\Delta N = 0, \Delta J = 1$ ($0000 \rightarrow 1001$) transition although the induced dipole moment coefficient A^{010} gives a two orders of magnitude larger dipole moment than the permanent dipole moment of free HD, as was discussed in [34]. This $\Delta J = 1$ transition in $HD@C_{60}$ is suppressed because there is an interference of two dipole terms, A^{010} and A^{101} which have opposite signs. The final state consists of 80% of the pure rotational state $J = 1, N = 0$ and 18% of the the pure translational state $N = 1, J = 0$. This mixed final state has matrix elements from the ground state for both A coefficients, A^{010} and A^{101} , which nearly cancel each other.

The observed low T IR transitions of H_2 , D_2 and $HD@C_{60}$ are collected in Table III. The content of the unperturbed $|JN\Lambda\rangle$ state in the final state is above $|\xi^1|^2 = 0.9$ in homonuclear species in most cases while for HD it varies and could be as low as 0.5. The mixing of states ξ^v is proportional to the energy separation of mixed states, $E_j - E_i$ in the first order perturbation theory. F_{00}^{00} couples states where $L_i = L_j$ and $J_i = J_j$. These states are far from each other as $L_i = L_j$ only if $N_j = N_i \pm 2$. The other term F_{00}^{22} mixes $L_j = L_i \pm 2$ and $J_j = J_i \pm 2$ what are even further from each other for small N . It was found by Xu et al. [41] that J is almost a good quantum number in H_2 and $D_2@C_{60}$ but not in $HD@C_{60}$. Indeed, the distance between states mixed decreases for HD as F_{00}^{11} mixes $L_j = L_i \pm 1$ and $J_j = J_i \pm 1$ and for this $N_j = N_i \pm 1$.

The vibrational frequency ω_0 is redshifted from its gas phase value for H_2 and D_2 , Table IV. The relative change of the frequency $[\omega_0(\text{gas}) - \omega_0(C_{60})]/\omega_0(\text{gas})$ depends on the cage and is independent of the hydrogen isotopomer [87]. Based on our fit results, Table IV, we get that for the H_2 $\omega_0(C_{60})/\omega_0(\text{gas}) = 0.9763$ and for the HD $\omega_0(C_{60})/\omega_0(\text{gas}) = 0.9773$. We used the average of these two ratios to calculate the $D_2@C_{60}$ fundamental vibrational frequency, $\omega_0 = 2924 \text{ cm}^{-1}$ what was necessary to fit the IR spectra to a model Hamiltonian [34]. At this point we cannot say how much of the redshift is caused by change in the zero-point vibrational energy and how much is caused by the change of anharmonic corrections to the vibrational levels in the C_{60} as our data set is limited to energy differences of $v = 0$ and $v = 1$ levels only. Note that the vibrational frequency of $H_2@C_{60}$ is $\omega_0 = 4062.4 \text{ cm}^{-1}$, Table IV, while the *para* vibrational transition is shifted up by

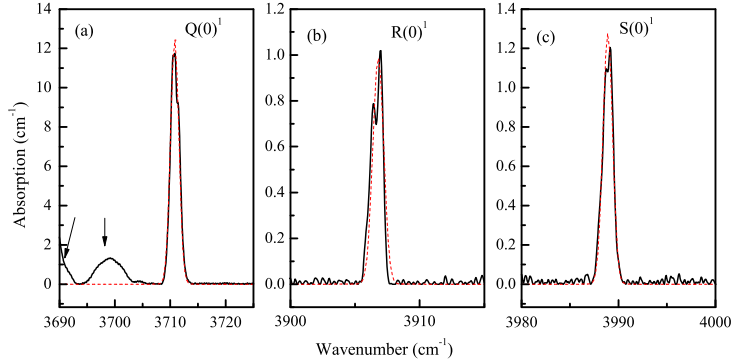


FIG. 7. Infrared absorption spectra of HD@C₆₀ at 5 K, black line. The parameters for the simulated spectrum (red line) are taken from the model fit of 90 K spectra [34]. The broad lines indicated by arrows are not due to HD. Line labels are the same as in Fig. 4b; superscript to line label shows the final state Λ . (Online version in Colour)

TABLE III. Experimental IR absorption line parameters of endohedral dihydrogen isotopologs in C₆₀ at 5 K. ω is the transition frequency in wavenumber units, cm⁻¹ and S is the integrated absorption line area in cm⁻² units. $JNLA$ are the quantum numbers of the main component with the weight $|\xi^1|^2$ in the final state $v = 1$. The $|\xi^0|^2$ of the main component $JNLA$ in the initial $v = 0$ state for H₂ are 0.97 of 0000 and 0.97 of 1001, for D₂ are 0.99 of 0000 and 0.99 of 1001, and for HD is 0.95 of 0000. Integrated absorption cross-section σ is used by some authors. The integrated line area S is transformed into σ (unit cm/molecule) using $\sigma = SV/\mathcal{N}$ where \mathcal{N} is the number of hydrogen molecules in the volume V [86]. Here $\mathcal{N}/V = 1.48 \times 10^{21}$ cm⁻³, the number density of molecules in solid C₆₀. * It was not possible to separate overlapping $Q(0)^1$ and $Q(1)^2$ lines of D₂ and the line area given is the sum of both transitions.

Line label	H ₂			D ₂			HD			Final state, $v = 1$
	ω	S	$ \xi^1 ^2$	ω	S	$ \xi^1 ^2$	ω	S	$ \xi^1 ^2$	$JNLA$
$Q(1)^1$	4065.4	0.093	0.98	–	–	0.99	–	–	0.80	1001
$Q(0)^0$	4071.4	0.011	0.98	–	–	0.99	–	–	0.96	0000
$Q(1)^1$	4244.5	5.76	0.95	3045.1	0.98	0.97	–	–	0.94	1111
$Q(1)^2$	4250.7	19.3	0.94	3050.2*	10.8	0.96	–	–	0.64	1112
$Q(0)^1$	4255.2	10.6	0.94	3050.2*	10.8	0.96	3710.8	23.5	0.73	0111
$Q(1)^0$	4261.0	8.86	0.94	3056.8	1.55	0.96	–	–	0.64	1110
$R(0)^1$	–	–	0.61	–	–	0.61	3906.7	1.05	0.50	1201
$S(0)^1$	4592.0	3.08	0.94	3224.35	1.66	0.96	3988.9	1.6	0.54	2111
$S(1)^1$	4612.5	0.3	0.97	–	–	0.96	–	–	0.58	3003
$S(1)^2$	4802.5	5.65	0.94	–	–	0.86	–	–	0.64	3112

9 cm⁻¹, to $\omega_0 = 4071.4$ cm⁻¹, Table III. This is because the zero-point translational energies are different in the $v = 0$ and $v = 1$ vibrational states [33].

The rotational constant B_e , the vibrational correction α_e , and the centrifugal correction D_e of the hydrogen inside C₆₀ and in free space are compared in Table IV. The smaller than the gas phase value of B_e may be interpreted as 0.8% (0.9%) stretching of the nucleus-nucleus distance s in H₂@C₆₀ (D₂@C₆₀), as $B_e \sim \langle 1/s^2 \rangle$. An attractive interaction between hydrogen atoms and the cage causes s to be longer. The elongation of the equilibrium proton-proton distance is consistent with the redshift of ω_0 [89]. However, the anharmonic vibrational correction to rotational constant, α_e , is smaller inside the cage than in the gas phase. Here the cage has the opposite, repulsive, effect and reduces the elongation of the proton-proton distance in the excited v states when compared to H₂ being in the free space. This is supported by the fact that within the error bars α_e of D₂@C₆₀ is equal to α_e of D₂. The vibrational amplitude of D₂ is less than of the H₂ and therefore the

TABLE IV. Values of the fitted parameters for $\text{H}_2@\text{C}_{60}$ [33] and for HD and $\text{D}_2@\text{C}_{60}$ [34]. The vibrational and rotational constants of a free molecule of the three hydrogen isotopologs are shown for comparison; gas phase ω_0 is calculated including all terms $(v + 1/2)^k$ up to $k = 3$ [88]. The parameter ${}^vV_{00}^{224}$ is set to zero for $\text{HD}@\text{C}_{60}$ and $\text{D}_2@\text{C}_{60}$. Parameter errors are given in [34].

κ_i	$\text{H}_2@\text{C}_{60}$		$\text{HD}@\text{C}_{60}$		$\text{D}_2@\text{C}_{60}$		Unit
	$v = 0$	$v = 1$	$v = 0$	$v = 1$	$v = 0$	$v = 1$	
${}^vV_{00}^{002}$	14.28	15.95	16.36	17.48	16.78	16.46	Jm^{-2}
${}^vV_{00}^{004}$	$2.21 \cdot 10^{21}$	$2.192 \cdot 10^{21}$	$1.88 \cdot 10^{21}$	$2.13 \cdot 10^{21}$	$2.16 \cdot 10^{21}$	$2.39 \cdot 10^{21}$	Jm^{-4}
${}^vV_{00}^{222}$	0.563	1.20	1.31	2.04	1.1	1.4	Jm^{-2}
${}^vV_{00}^{224}$	$2.21 \cdot 10^{20}$	$1.03 \cdot 10^{20}$	0	0	0	0	Jm^{-4}
${}^vV_{00}^{111}$	—	—	$3.11 \cdot 10^{-10}$	$3.25 \cdot 10^{-10}$	—	—	Jm^{-1}
${}^vV_{00}^{113}$	—	—	$4.3 \cdot 10^{10}$	$7.1 \cdot 10^{10}$	—	—	Jm^{-3}
n_o/n_p	2.89	—	—	—	2	—	Cm
A^{010}	—	—	$-1.5 \cdot 10^{-32}$	—	—	—	C
A^{101}	$9.1 \cdot 10^{-22}$	—	$7.0 \cdot 10^{-22}$	—	$6.9 \cdot 10^{-22}$	—	C
A^{121}	$-4.3 \cdot 10^{-22}$	—	$-2.7 \cdot 10^{-22}$	—	$-2.9 \cdot 10^{-22}$	—	C
	$\text{H}_2@\text{C}_{60}$	H_2	$\text{HD}@\text{C}_{60}$	HD	$\text{D}_2@\text{C}_{60}$	D_2	
ω_0	4062.4	4161.18	3549.7	3632.20	2924	2993.69	cm^{-1}
B_e	59.87	60.853	45.4	45.655	29.89	30.444	cm^{-1}
α_e	2.97	3.062	1.70	1.986	1.09	1.079	cm^{-1}
D_e	$4.83 \cdot 10^{-2}$	$4.71 \cdot 10^{-2}$	$1.5 \cdot 10^{-1}$	$2.605 \cdot 10^{-2}$	$8 \cdot 10^{-3}$	$1.141 \cdot 10^{-2}$	cm^{-1}

repulsive effect of the cage becomes important at $v > 1$ for D_2 .

Among the rotational and vibrational constants of $\text{HD}@\text{C}_{60}$ the centrifugal correction D_e to the rotational constant is anomalously different from its gas phase value compared to other two isotopomers, Table IV. Positive D_e means that the faster the molecule rotates, the longer is the bond. We speculate that since the rotation center of HD inside the cage is further away from the deuteron, the centrifugal force on the deuteron increases and the bond is stretched more than in the free HD molecule.

A similar system to the one studied here is exohedral H_2 in C_{60} . There H_2 occupies the octahedral interstitial site in the C_{60} crystal. The prominent features in the exohedral H_2 IR spectra [56] are the translational, $\Delta N = \pm 1$, sidebands to the fundamental transitions, $\Delta v = 1$ and $\Delta J = 0, 2$. The redshift of the fundamental vibrational frequency is about 60 cm^{-1} , which is less than in $\text{H}_2@\text{C}_{60}$ where it is 98.8 cm^{-1} . Also the separation of translational $N = 0$ and $N = 1$ levels, approximately 120 cm^{-1} , is smaller, when compared to 184.4 cm^{-1} in $\text{H}_2@\text{C}_{60}$. It is likely that the main contribution to the latter difference comes from the larger van der Waals volume available for H_2 in the octahedral site than in the C_{60} cage.

$\text{H}_2@\text{C}_{70}$

IR absorption spectra of $\text{H}_2@\text{C}_{70}$ measured at 5 K are shown in Fig. 8 and the scheme of energy levels with the low T transitions indicated with arrows is shown in Fig. 9. The transitions where $\Delta J = 0$ and the translational state changes by $\Delta n = 1$ or $\Delta n_z = 1$ are labeled as $Q_{xy}(J)$ and $Q_z(J)$ where J is the rotational quantum number of the initial state. The transitions where $\Delta J = 2$ are labeled by $S_{xy}(J)$ and $S_z(J)$. The z and xy translational modes have distinctly different energies. For the Q lines they are shown in different panels, Fig. 8 a and 8 b. The *para* and *ortho* S lines are well separated because of different rotational energies. The *para* S lines are shown in Fig. 8 c and *ortho* S lines are shown in Fig. 8 d. The Q lines cannot be sorted out into *para* and *ortho* that easily. An exception is the $Q(1)$ transition, inset to Fig. 8 a. This is a pure vibrational transition, $v = 0 \rightarrow 1$, without the change of translational or rotational states. The corresponding

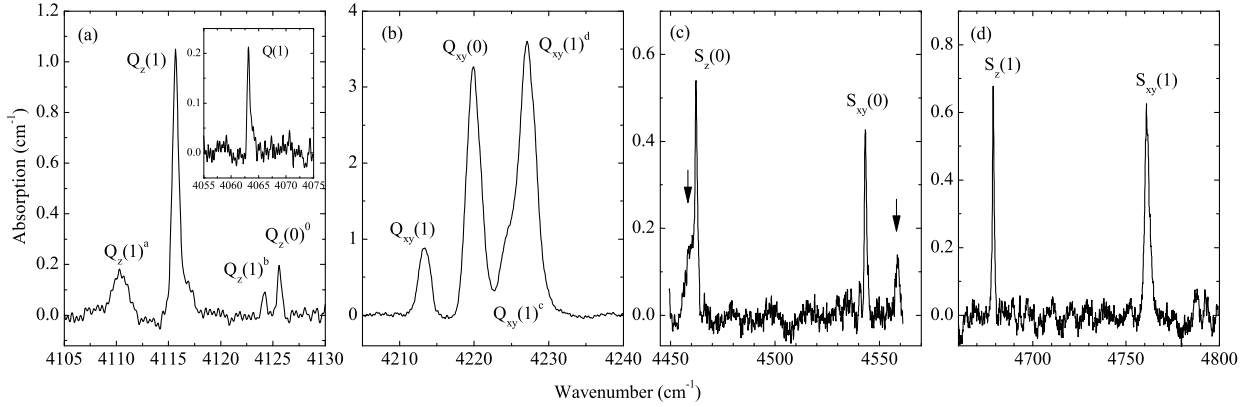


FIG. 8. IR absorption spectra of $\text{H}_2@C_{70}$ at 5 K. Features shown with arrows in panel (c) are likely caused by impurities, not by endohedral H_2 .

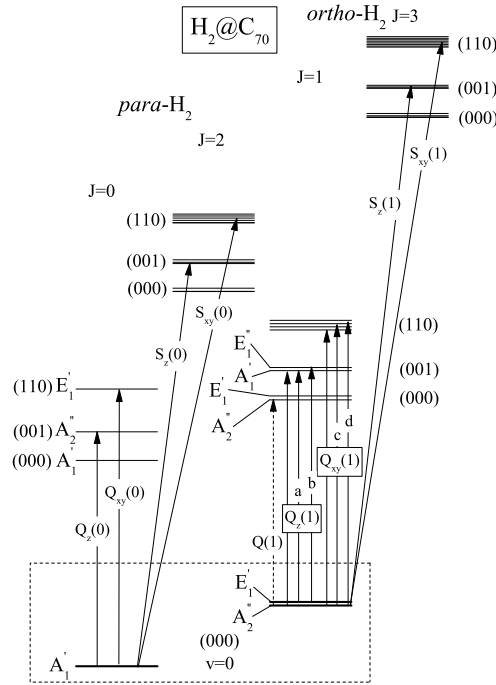


FIG. 9. Energy levels and observed IR transitions of $\text{H}_2@C_{70}$ from the ground *para* and *ortho* translational states in the $v = 0$ state to the excited vibrational state $v = 1$. The irreducible representations of the symmetry group D_{5h} are given for few lower states and are listed in Table II. The ordering of the states is based on [41]. *ortho*- H_2 transitions marked by a and b are $Q_z(1)^a$ and $Q_z(1)^b$ in Table V and start from the thermally excited state, which is E_1' (000) according to [41]. There are three experimentally observed *ortho*- H_2 transitions from the ground A_2'' (000) state: $Q_{xy}(1)$, $Q_{xy}(1)^c$, and $Q_{xy}(1)^d$.

(fundamental) *para* transition $Q(0)$ would be at 4069.3 cm^{-1} according to the model, Table V. We expect it to be much weaker than the *ortho* $Q(1)$ transition, as in $\text{H}_2@C_{60}$, and for this reason it is not observed in the experiment.

In Fig. 10 we plot the normalized line area and normalized Boltzmann population. Fig. 10 a shows the T dependence of *para* lines. The assignment of the 4125.6 cm^{-1} line to $Q_z(0)$ and the 4219.9 cm^{-1} line to $Q_{xy}(0)$ is supported by our model that is summarized in Table V and will be

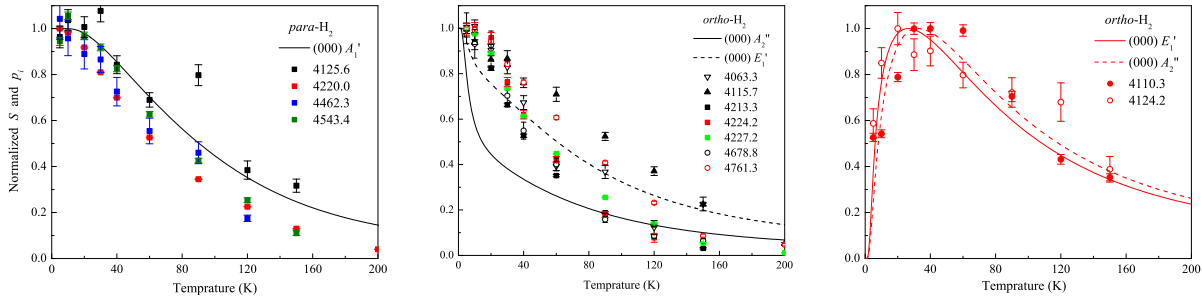


FIG. 10. Normalized line area and Boltzmann population of *para* and *ortho* transitions of $\text{H}_2@C_{70}$ starting from the ground translational state. (a) *para* lines, (b) and (c) *ortho* lines. Solid line in (b) is the normalized intensity when the initial state is the ground state A_2'' ($J_z = 0$) and in (c) when the initial state is E_1' ($J_z = \pm 1$), 7 cm^{-1} above A_2'' . This corresponds to ${}^0\kappa > 0$, Eq. 13. Dashed line in (b) and (c) is the reversed situation when the ground state is doubly degenerate E_1' and A_2'' is 7 cm^{-1} above it, i.e. ${}^0\kappa < 0$. The normalized intensities are calculated using the translational energy levels from the 5D quantum mechanical calculation [41] and Eq. 20.

discussed below.

The uniaxial symmetry of C_{70} splits the *ortho* ground state $J = 1$. This splitting is about $7 \text{ cm}^{-1} \approx 10 \text{ K}$ and creates a sharp T dependence of the *ortho* line intensity at low T as is shown in Fig. 2. This feature could be used to determine which of the Q lines belong to the *ortho* species. Two lines, 4110.5 cm^{-1} and 4124.2 cm^{-1} , have a T dependence consistent with the *ortho* transitions starting from the ground translational (000) state of E_1' symmetry, Fig. 10 a. However, according to our model there is no transition close to 4124.2 cm^{-1} from the thermally excited *ortho* E_1' state, Table V. This might be due to our simplified model where the rotational anisotropy parameter ${}^v\kappa$ is assumed equal in $v = 0$ and $v = 1$ vibrational states. The rest of the *ortho* lines are shown in Fig. 10 b. Several lines follow the same T dependence, the fundamental transition at 4063.2 cm^{-1} , $Q_{xy}(1)$ lines 4213.4 , 4224.7 , and 4226.9 cm^{-1} and the $S_z(1)$ line at 4678.8 cm^{-1} . Lines $Q_z(1)$ at 4116 and $S_{xy}(1)$ at 4761 cm^{-1} have distinctly different T dependence than the rest of the lines. Such deviation could be due to the overlap of transitions starting from A_2'' and E_1' symmetry states. However, none of the *ortho* lines behaves like the theoretical prediction, black line, so the possibility that the ground *ortho* state is doubly degenerate E_1' and not the A_2'' , i.e. ${}^0\kappa < 0$, is not ruled out by our data. The dashed black line shows the ground state population if the ground state is E_1' and the A_2'' state is 7 cm^{-1} above it. This T dependence is more close to the experimental situation than the solid black line, where ${}^0\kappa > 0$. The change of sign of ${}^0\kappa$ affects intensities only a little if the transitions start from the thermally excited state, Fig. 10 c, where the red dashed line is the normalized Boltzmann population of A_2'' state if this state is 7 cm^{-1} above the ground state E_1' , i.e. if ${}^0\kappa < 0$.

It is not unreasonable that ${}^0\kappa < 0$ and the E_1' ($J_z = \pm 1$) state is the ground rotational state of *ortho*- H_2 . It requires that there is an attraction instead of repulsion between H and C when H_2 is in the center of the C_{70} cage. The attraction is stronger for the H_2 if its molecular axis is in the xy plane, $J_z = \pm 1$, where the distance between H and C is less than if the axis is along the z , $J_z = 0$, where the H-C distance is longer. Indeed, the attraction between C and H in $\text{H}_2@C_{60}$ was deduced from the redshift of vibrational energy and reduced rotational constant compared to H_2 in the gas phase [33]. However, it was found by 5D quantum mechanical calculation that A_2'' is the ground state [41]. More elaborate model with dipole moment parameters that describe the IR line intensities together with the Boltzmann population could resolve the issue.

Table V summarizes the assignment of transitions observed in the experiment. Since our model described in Section did not include translation-rotation coupling we used the transitions where L

TABLE V. Low temperature IR transitions of $\text{H}_2@C_{70}$ observed at 5K from the ground vibrational state $v = 0$ to the excited vibrational state $v = 1$. $J(nln_z)$ are the quantum numbers for the initial and final states and the labels indicate corresponding transitions in Fig. 8 and 9. The experimental spectra were fitted with Gaussians, S_{exp} is the experimental line area; the experimental line position ω_{exp} could always be determined with a precision better than 0.1 cm^{-1} . The model parameters, Eq.14, were determined as described in the text by matching the model frequency ω_{mod} to the experimental frequency ω_{exp} for four lines indicated with error $\mathbf{0}$. The model parameters are vibrational frequency $\omega_0 = 4069.1 \text{ cm}^{-1}$, 1D oscillator frequency along the z axis $\nu\omega_z^T = 56.5 \text{ cm}^{-1}$, 2D circular oscillator frequency $\nu\omega_{xy}^T = 150.9 \text{ cm}^{-1}$, and the rotational anisotropy parameter $\nu\kappa = 3.1 \text{ cm}^{-1}$. The rotational constant $B_e = 59.865 \text{ cm}^{-1}$ and its corrections, $\alpha_e = 2.974 \text{ cm}^{-1}$ and $D_e = 0.04832 \text{ cm}^{-1}$ were assumed to be the same as in $\text{H}_2@C_{60}$.

Frequency (cm^{-1})		S_{exp} (cm^{-2})	Initial $v = 0$		Final $v = 1$		Label	Error (cm^{-1})
ω_{exp}	ω_{mod}		J	(nln_z)	J	(nln_z)		$\omega_{exp} - \omega_{mod}$
4063.2	4063.2	0.146 ± 0.005	1	(000)	1	(000)	$Q(1)$	$\mathbf{0}$
–	4069.1	–	0	(000)	1	(000)	$Q(0)$	–
4110.3	4110.3	0.311 ± 0.014	1	(000)	1	(001)	$Q_z(1)^a$	$\mathbf{0}$
4115.7	4119.7	0.824 ± 0.009	1	(000)	1	(001)	$Q_z(1)$	-4.0
4124.2	4119.7	0.045 ± 0.007	1	(000)	1	(001)	$Q_z(1)^b$	4.5
4125.6	4125.6	0.096 ± 0.007	0	(000)	0	(001)	$Q_z(0)$	$\mathbf{0}$
4213.3	4214.1	1.759 ± 0.024	1	(000)	1	(110)	$Q_{xy}(1)$	-0.8
4220.0	4220.0	7.702 ± 0.027	0	(000)	0	(110)	$Q_{xy}(0)$	$\mathbf{0}$
4224.2	4214.1	2.111 ± 0.066	1	(000)	1	(110)	$Q_{xy}(1)^c$	10.1
4227.2	4214.1	10.143 ± 0.067	1	(000)	1	(110)	$Q_{xy}(1)^d$	13.1
4462.3	4456.3	0.570 ± 0.023	0	(000)	2	(001)	$S_z(0)$	6.0
4543.4	4550.7	0.582 ± 0.012	0	(000)	2	(110)	$S_{xy}(0)$	-7.3
4678.8	4667.0	0.831 ± 0.012	1	(000)	3	(001)	$S_z(1)$	11.8
4761.3	4761.3	1.900 ± 0.019	1	(000)	3	(110)	$S_{xy}(1)$	0.0

and J are both zero or one of them is zero in the initial and final states. The fundamental frequency $\omega_0 = 4069.1 \text{ cm}^{-1}$ was chosen to match the experimental fundamental *ortho* transition $Q(1)$; the rotational constant $B_e = 59.865 \text{ cm}^{-1}$ and its corrections $\alpha_e = 2.974 \text{ cm}^{-1}$, $D_e = 0.04832 \text{ cm}^{-1}$ of $\text{H}_2@C_{60}$ were used. Next the two *para* transitions were matched, $Q_z(0)$ and $Q_{xy}(0)$ to obtain $\nu\omega_z^T = 56.5 \text{ cm}^{-1}$, $\nu\omega_{xy}^T = 150.9 \text{ cm}^{-1}$. The 4220 cm^{-1} line was chosen as $Q_{xy}(0)$ because its T dependence, Fig. 10 a), is similar to $S_z(0)$ and $S_{xy}(0)$ line T dependence. The *ortho* ground state splitting is 9.4 cm^{-1} (7.4 cm^{-1} from the 5D calculation [41]) with $\nu\kappa = 3.1 \text{ cm}^{-1}$ which was obtained by assuming that the $Q_z(1)^a$ transition, $(000)E'_1 \rightarrow (001)A'_1$ in Fig. 9, is centered at 4110.3 cm^{-1} . It was assumed that the anharmonic corrections to translational energy and to $\nu\kappa$ are same for the $v = 0$ and $v = 1$ vibrational states.

The variation of the experimental frequencies compared to the model frequencies is within $\pm 10 \text{ cm}^{-1}$, Table V. This is reasonable since our model did not include translation-rotation coupling and the translation-rotation coupling in $\text{H}_2@C_{60}$ creates splittings of this magnitude. The vibrational frequency ω_0 is larger in $\text{H}_2@C_{70}$ than in $\text{H}_2@C_{60}$. This difference must be taken with a reservation because the correction due to the difference of zero point translational energies in two vibrational states is not taken into account for $\text{H}_2@C_{70}$ as it was done for $\text{H}_2@C_{60}$ [33]. Again, a more elaborate model is needed for C_{70} than the two oscillator model described in Section.

CONCLUSIONS

IR absorption spectra of endohedral hydrogen isotopologs, H₂ [32, 33], D₂ [34], and HD [34] in C₆₀ are informative, involving excitations of vibrations, rotations and translational motion of dihydrogen. The translational motion of the encapsulated molecule is quantized and coupled to its rotations because of the surrounding C₆₀ cage. The vibrational frequency of dihydrogen is redshifted compared to the gas phase value. Together with the smaller rotational constant it shows that the hydrogen bond is stretched inside the cage and there is an attraction between H (or D) and C. The heteronuclear HD does not rotate about its center of mass because of the surrounding cage. Different rotational and translational states are mixed and rotational quantum number J is not a good quantum number for HD@C₆₀.

Our study shows that the vibrations and rotations of C₆₀ and the crystal field effects of solid C₆₀ are not important on the energy scale of IR measurements. If these effects are important their contribution to the IR spectra is the order of one wavenumber splitting of few absorption lines. Such small splitting is consistent with the NMR [28, 29] and heat capacity [30] results.

C₇₀ has ellipsoidal shape and this splits the translation-rotation states of H₂. The translational frequency is about 180 cm⁻¹ in H₂@C₆₀. In C₇₀ this three dimensional mode is split into a two dimensional mode at 151 cm⁻¹ and a one dimensional mode at 56 cm⁻¹. The 5D quantum mechanical calculation [41] is in very good agreement with this experimental result.

ACKNOWLEDGMENTS

This research was supported by the Estonian Ministry of Education and Research grant SF0690029s09, Estonian Science Foundation grants ETF8170, ETF8703, JD187.

* toomas.room@kbfi.ee

- [1] H. Kroto, J. Heath, S. O'Brian, R. F. Curl, and R. E. Smalley, *Nature* **318**, 162 (1985).
- [2] J. R. Heath, S. C. O'Brien, Q. Zhang, Y. Liu, R. F. Curl, F. K. Tittel, and R. E. Smalley, *Journal of the American Chemical Society* **107**, 7779 (1985),
- [3] M. Saunders, H. A. Jiménez-Vázquez, R. J. Cross, and R. J. Poreda, *Science* **259**, 1428 (1993),
- [4] M. Saunders, H. A. Jimenez-Vazquez, R. J. Cross, S. Mroczkowski, M. L. Gross, D. E. Giblin, and R. J. Poreda, *J. Am. Chem. Soc.* **116**, 2193 (1994),
- [5] H. Mauser, A. Hirsch, N. J. R. van Eikema Hommes, T. Clark, B. Pietzak, A. Weidinger, and L. Dunsch, *Angew. Chem., Int. Ed.* **36**, 2835 (1997), ISSN 1521-3773.
- [6] J. A. Larsson, J. C. Greer, W. Harneit, and A. Weidinger, *J. Chem. Phys.* **116**, 7849 (2002).
- [7] L. Dunsch and S. Yang, *small* **3**, 12981320 (2007).
- [8] Y. Rubin, *Chem.–Eur. J.* **3**, 1009 (1997), ISSN 1521-3765.
- [9] Y. Rubin, T. Jarrosson, G.-W. Wang, M. D. Bartberger, K. N. Houk, G. Schick, M. Saunders, and R. J. Cross, *Angew. Chem. Int. Ed.* **40**, 1543 (2001).
- [10] Y. Murata, M. Murata, and K. Komatsu, *J. Am. Chem. Soc.* **125**, 7152 (2003).
- [11] K. Komatsu, M. Murata, and Y. Murata, *Science* **307**, 238 (2005).
- [12] M. Murata, Y. Murata, and K. Komatsu, *J. Am. Chem. Soc.* **128**, 8024 (2006).
- [13] Y. Murata, S. Maeda, M. Murata, and K. Komatsu, *J. Am. Chem. Soc.* **130**, 6702 (2008), ISSN 0002-7863.
- [14] M. Murata, S. Maeda, Y. Morinaka, Y. Murata, and K. Komatsu, *J. Am. Chem. Soc.* **130**, 15800 (2008).
- [15] S. Iwamatsu, C. Stanisky, R. J. Cross, M. Saunders, N. Mizorogi, S. Nagase, and S. Murata, *Angew. Chem. Int. Ed.* **45**, 5337 (2006).

- [16] S.-I. Iwamatsu, T. Uozaki, K. Kobayashi, S. Re, S. Nagase, and S. Murata, *J. Am. Chem. Soc.* **126**, 2668 (2004),
- [17] Z. Xiao, J. Yao, D. Yang, F. Wang, S. Huang, L. Gan, Z. Jia, Z. Jiang, X. Yang, B. Zheng, et al., *J. Am. Chem. Soc.* **129**, 16149 (2007),
- [18] K. E. Whitener, M. Frunzi, S.-i. Iwamatsu, S. Murata, R. J. Cross, and M. Saunders, *J. Am. Chem. Soc.* **130**, 13996 (2008), pMID: 18817388,
- [19] K. E. Whitener, R. J. Cross, M. Saunders, S.-I. Iwamatsu, S. Murata, N. Mizorogi, and S. Nagase, *J. Am. Chem. Soc.* **131**, 6338 (2009), pMID: 19368384,
- [20] K. Kurotobi and Y. Murata, *Science* **333**, 613 (2011),
- [21] C. Beduz, M. Carravetta, J. Y.-C. Chen, M. Concistré, M. Denning, M. Frunzi, A. J. Horsewill, O. G. Johannessen, R. Lawler, X. Lei, et al., *Proc. Natl. Acad. Sci. U. S. A.* **109**, 12894 (2012).
- [22] E. Sartori, M. Ruzzi, N. J. Turro, J. D. Decatur, D. C. Doetschman, R. G. Lawler, A. L. Buchachenko, Y. Murata, and K. Komatsu, *J. Am. Chem. Soc.* **128**, 14752 (2006).
- [23] J. Y.-C. Chen, A. A. Marti, N. J. Turro, K. Komatsu, Y. Murata, and R. G. Lawler, *The Journal of Physical Chemistry B* **114**, 14689 (2010),
- [24] E. Sartori, M. Ruzzi, N. Turro, K. Komatsu, Y. Murata, R. Lawler, and A. Buchachenko, *J. Am. Chem. Soc.* **130**, 2221 (2008).
- [25] M. Frunzi, X. Lei, Y. Murata, K. Komatsu, S.-I. Iwamatsu, S. Murata, R. G. Lawler, and N. J. Turro, *J. Phys. Chem. Lett.* **1**, 1420 (2010),
- [26] N. J. Turro, A. A. Marti, J. Y.-C. Chen, S. Jockusch, R. G. Lawler, M. Ruzzi, E. Sartori, S.-C. Chuang, K. Komatsu, and Y. Murata, *J. Am. Chem. Soc.* **130**, 10506 (2008).
- [27] M. Frunzi, S. Jockusch, J. Y.-C. Chen, R. M. K. Calderon, X. Lei, Y. Murata, K. Komatsu, D. M. Guldi, R. G. Lawler, and N. J. Turro, *J. Am. Chem. Soc.* **133**, 14232 (2011),
- [28] M. Carravetta, O. G. Johannessen, M. H. Levitt, I. Heinmaa, R. Stern, A. Samoson, A. J. Horsewill, Y. Murata, and K. Komatsu, *J. Chem. Phys.* **124**, 104507 (2006).
- [29] M. Carravetta, A. Danquigny, S. Mamone, F. Cuda, O. G. Johannessen, I. Heinmaa, K. Panesar, R. Stern, M. C. Grossel, A. J. Horsewill, et al., *Phys. Chem. Chem. Phys.* **9**, 4879 (2007).
- [30] Y. Kohama, T. Rachi, J. Jing, Z. Li, J. Tang, R. Kumashiro, S. Izumisawa, H. Kawaji, T. Atake, H. Sawa, et al., *Phys. Rev. Lett.* **103**, 073001 (2009).
- [31] S. Mamone, J. Y.-C. Chen, R. Bhattacharyya, M. H. Levitt, R. G. Lawler, A. J. Horsewill, T. Rõõm, Z. Bačić, and N. J. Turro, *Coordination Chemistry Reviews* **255**, 938 (2011).
- [32] S. Mamone, M. Ge, D. Hüvonen, U. Nagel, A. Danquigny, F. Cuda, M. C. Grossel, Y. Murata, K. Komatsu, M. H. Levitt, et al., *J. Chem. Phys.* **130**, 081103 (2009).
- [33] M. Ge, U. Nagel, D. Hüvonen, T. Rõõm, S. Mamone, M. H. Levitt, M. Carravetta, Y. Murata, K. Komatsu, J. Y.-C. Chen, et al., *J. Chem. Phys.* **134**, 054507 (2011).
- [34] M. Ge, U. Nagel, D. Hüvonen, T. Rõõm, S. Mamone, M. H. Levitt, M. Carravetta, Y. Murata, K. Komatsu, X. Lei, et al., *J. Chem. Phys.* **135**, 114511 (2011), ISSN 00219606.
- [35] A. J. Horsewill, S. Rols, M. R. Johnson, Y. Murata, M. Murata, K. Komatsu, M. Carravetta, S. Mamone, M. H. Levitt, J. Y.-C. Chen, et al., *Phys. Rev. B* **82**, 081410 (2010).
- [36] P. M. Rafailov, C. Thomsen, A. Bassil, K. Komatsu, and W. Bacsá, *Phys. Stat. Sol. (b)* **242**, R106 (2005).
- [37] J. M. Brown and A. Carrington, *Rotational Spectroscopy of Diatomic Molecules* (Cambridge Uni. Press, 2003).
- [38] N. J. Turro, J. Y. C. Chen, M. Sartori, E.; Ruzzi, A. A. Marti, R. G. Lawler, S. Jockusch, J. Lpez-Gejo, K. Komatsu, and Y. Murata, *Accounts of Chemical Research* **43**, 335 (2010).
- [39] M. Xu, F. Sebastianelli, Z. Bačić, R. Lawler, and N. J. Turro, *J. Chem. Phys.* **128**, 011101 (2008).
- [40] M. Xu, F. Sebastianelli, Z. Bačić, R. Lawler, and N. J. Turro, *J. Chem. Phys.* **129**, 064313 (2008).
- [41] M. Xu, F. Sebastianelli, B. R. Gibbons, Z. Bačić, R. Lawler, and N. J. Turro, *J. Chem. Phys.* **130**, 224306 (2009).
- [42] T. B. Lee and M. L. McKee, *JACS* **130**, 17610 (2008),
- [43] F. Sebastianelli, M. Xu, Z. Bačić, R. Lawler, and N. J. Turro, *JACS* **132**, 9826 (2010).
- [44] H. Erkol and E. Demiralp, *Mol. Phys.* **107**, 2053 (2009),
- [45] G. A. Dolgonos and G. H. Peslherbe, *Chem. Phys. Lett.* **513**, 236 (2011), ISSN 0009-2614.
- [46] G. Jiménez-Osés, J. I. Garcíá, F. Corzana, and J. Elguero, *Org. Lett.* **13**, 2528 (2011),
- [47] W. H. Shaffer, *Rev. Mod. Phys.* **16**, 245 (1944).

- [48] S. Flügge, *Practical Quantum Mechanics*, vol. 1 (Springer-Verlag (Berlin), 1971).
- [49] R. J. Cross, *J. Phys. Chem. A* **105**, 6943 (2001).
- [50] T. Yildirim and A. B. Harris, *Phys. Rev. B* **66**, 214301 (2002).
- [51] M. Krause, M. Hulman, H. Kuzmany, O. Dubay, G. Kresse, K. Vietze, G. Seifert, C. Wang, and H. Shinohara, *Phys. Rev. Lett.* **93**, 137403 (2004).
- [52] K. H. Michel, B. Verberck, M. Hulman, H. Kuzmany, and M. Krause, *J. Chem. Phys.* **126**, 064304 (2007).
- [53] A. P. Smith, R. Benedek, F. R. Trouw, M. Minkoff, and L. H. Yang, *Phys. Rev. B* **53**, 10187 (1996).
- [54] L. Bengtsson, K. Svensson, M. Hassel, J. Bellman, M. Persson, and S. Andersson, *Phys. Rev. B* **61**, 16921 (2000).
- [55] S. A. FitzGerald, S. Forth, and M. Rinkoski, *Phys. Rev. B* **65**, 140302 (2002).
- [56] S. A. FitzGerald, H. O. H. Churchill, P. M. Korngut, C. B. Simmons, and Y. E. Strangas, *Phys. Rev. B* **73**, 155409 (2006).
- [57] A. I. Kolesnikov, V. E. Antonov, I. O. Bashkin, G. Grosse, A. P. Moravsky, A. Y. Muzychka, E. G. Ponyatovsky, and F. E. Wagner, *J. Phys.: Condens. Matter* **9**, 2831 (1997).
- [58] S. A. FitzGerald, T. Yildirim, L. J. Santodonato, D. A. Neumann, J. R. D. Copley, J. J. Rush, and F. Trouw, *Phys. Rev. B* **60**, 6439 (1999).
- [59] M. Tomaselli and B. H. Meier, *J. Chem. Phys.* **115**, 11017 (2001).
- [60] M. Tomaselli, *Mol. Phys.* **101**, 3029 (2003).
- [61] K. A. Williams, B. K. Pradhan, P. C. Eklund, M. K. Kostov, and M. W. Cole, *Phys. Rev. Lett.* **88**, 165502 (2002).
- [62] R. M. Herman and J. C. Lewis, *Phys. Rev. B* **73**, 155408 (2006).
- [63] E. H. T. Olthof, A. van der Avoird, and P. E. S. Wormer, *J. Chem. Phys.* **104**, 832 (1996).
- [64] C. Cohen-Tannoudji, B. Diu, and F. Laloë, *Quantum Mechanics* (Wiley-VCH, 1977).
- [65] G. Herzberg, *Molecular spectra and molecular structure, I. Spectra of diatomic molecules* (Van Nostrand Company, Inc. (Princeton), 1950), 2nd ed.
- [66] J. L. Dunham, *Phys. Rev.* **41**, 721 (1932).
- [67] S. L. Altmann and P. Herzog, *Point-Group Theory Tables* (Oxford University Press, Oxford, 1994).
- [68] W. Gordy and R. L. Cook, *Microwave Molecular Spectra*, vol. 18 of *Techniques of Chemistry* (Wiley-Interscience, New York, 1984), 3rd ed.
- [69] K. Hedberg, L. Hedberg, M. Bühl, D. S. Bethune, C. A. Brown, and R. D. Johnson, *J. Am. Chem. Soc.* **119**, 5314 (1997).
- [70] K. Hedberg, L. Hedberg, D. S. Bethune, C. A. Brown, H. C. Dorn, R. D. Johnson, and M. de Vries, *Science* **254**, 410 (1991).
- [71] T. Yildirim and A. B. Harris, *Phys. Rev. B* **67**, 245413 (2003).
- [72] E. J. Allin, W. F. J. Hare, and R. E. MacDonald, *Phys. Rev.* **98**, 554 (1955).
- [73] W. F. J. Hare, E. J. Allin, and H. L. Welsh, *Phys. Rev.* **99**, 1887 (1955).
- [74] B. Hourahine and R. Jones, *Phys. Rev. B* **67**, 121205 (2003).
- [75] A. Kudian and M. Welsh, *Can. J. Phys.* **49**, 230 (1971).
- [76] A. R. W. McKellar and H. L. Welsh, *Can. J. Phys.* **52**, 1082 (1974).
- [77] E. E. Chen, M. Stavola, W. B. Fowler, and P. Walters, *Phys. Rev. Lett.* **88**, 105507 (2002).
- [78] T. Oka, *Annu. Rev. Phys. Chem.* **44**, 299 (1993).
- [79] L. Frommhold, *Collision-Induced Absorption in Gases*, vol. 2 of *Cambridge Monographs on Atomic, Molecular, and Chemical Physics* (Cambridge University Press, Cambridge, 1993).
- [80] R. M. Berns, P. E. S. Wormer, F. Mulder, and A. van der Avoird, *J. Chem. Phys.* **69**, 2102 (1978).
- [81] P. E. S. Wormer and G. V. Dijk, *J. Chem. Phys.* **70**, 5695 (1979).
- [82] W. Meyer and L. Frommhold, *Phys. Rev. A* **34**, 2771 (1986).
- [83] L. Frommhold and W. Meyer, *Phys. Rev. A* **35**, 632 (1987).
- [84] M. Gustafsson, L. Frommhold, and W. Meyer, *J. Chem. Phys.* **113**, 3641 (2000).
- [85] C. C. Homes, P. J. Horoyski, M. L. W. Thewalt, and B. P. Clayman, *Phys. Rev. B* **49**, 7052 (1994).
- [86] R. Loudon, *The Quantum Theory of Light* (Oxford University Press, London - New York - Toronto, 1983), 2nd ed.
- [87] A. D. Buckingham, *Trans. Faraday Soc.* **56**, 753 (1960).
- [88] K. P. Huber and G. Herzberg, *Constants of Diatomic Molecules*, vol. IV of *Molecular Spectra and Molecular Structure* (Van Nostrand Reinhold Company, New York, 1979).

[89] C. G. Van de Walle, Phys. Rev. Lett. **80**, 2177 (1998).